Nuclear Physics **A510** (1990) 503-517
North-Holland

THE LEVEL STRUCTURE OF ^{20}Na AND THE IMPACT UPON THE STELLAR REACTION RATE FOR ^{19}Ne(p, γ)^{20}Na

L.O. LAMM, C.P. BROWNE, J. GÖRRES, S.M. GRAFF and M. WIESCHER

Department of Physics, University of Notre Dame, Notre Dame, IN 46556, USA

A.A. ROLLEFSON

Department of Physics and Astronomy, University of Arkansas, Little Rock, AR 72204, USA

B.A. BROWN

National Superconducting Cyclotron Laboratory
and Department of Physics and Astronomy
Michigan State University, East Lansing, MI 48824, USA

Received 12 September 1989
(Revised 13 November 1989)

Abstract: The level structure of ^{20}Na up to 3.6 MeV excitation energy has been investigated via the ^{20}Ne(^{3}He, t)^{20}Na charge exchange reaction. The observed bound and unbound states are discussed in terms of the analog structure of the $A = 20$, $T = 1$ triplet. The partial widths of the unbound levels have been calculated to derive the resonance strengths of these states in the ^{19}Ne(p, γ)^{20}Na reaction channel. The stellar reaction rate for ^{19}Ne(p, γ)^{20}Na has been calculated and is compared with previous estimates.

E

NUCLEAR REACTIONS ^{20}Ne(^{3}He, t), $E = 25.5$ MeV; measured $\sigma(\theta)$. ^{20}Na deduced levels, J, π. ^{19}Ne(p, γ), E = low; calculated stellar reaction rate.

1. Introduction

Nucleosynthesis in hot hydrogen burning is determined by the hot CNO cycle [1]) and, at temperatures $T_9 > 0.1$, by the rp process [2]). Reaction flow studies [2,3]) indicate that these two processes are linked by the reaction sequence ^{15}O(α, γ)^{19}Ne(p, γ)^{20}Na. Through this reaction link, CNO material is made available to the rp process for processing towards the Fe-Ni region. The ^{15}O(α, γ)^{19}Ne reaction has recently been studied, both theoretically [2,4]) and experimentally [5]), and its reaction rate seems to be well understood. The reaction rate for ^{19}Ne(p, γ)^{20}Na is, however, largely uncertain. Recent theoretical estimates [2,4]), have been based either on insufficient experimental information about the level structure of the compound nucleus ^{20}Na [ref. [6])] or on level energies calculated from the Thomas-Ehrman shift of known states in the mirror nucleus ^{20}F. Both results indicate that no resonances are expected at proton energies below 700 keV. On the basis of these results it has been argued that at lower temperatures the stellar reaction rate is dominated by nonresonant processes.

Until recently, very little experimental information was available about the nuclear structure of ^{20}Na above the proton threshold [7]). In a first attempt to investigate proton unbound states in ^{20}Na using the ^{20}Ne(^{3}He, t)^{20}Na charge exchange reaction [8]) several new levels were tentatively identified. These measurements, however, suffered from experimental shortcomings, including insufficient particle identification in the detector system, significant contamination of the target gas with oxygen, and poor statistics due to small beam currents. In this work we will report the final results of the study of the ^{20}Na nucleus via the ^{20}Ne(^{3}He, t)^{20}Na reaction, which was undertaken after the experimental problems discussed above were eliminated. We will compare our results with those of a recent study of ^{20}Ne(^{3}He, t)^{20}Na and ^{20}Ne(p, n)^{20}Na [ref. [9])] as well as with shell-model calculations for ^{20}Na. We will discuss spin and parity assignments for the observed levels and will evaluate the possible impact of these states upon the stellar reaction rate for ^{19}Ne(p, γ)^{20}Na.

2. Experimental equipment and procedure

The experiment was performed with the FN-Tandem accelerator at the Nuclear Structure Laboratory of the University of Notre Dame. The ^{20}Ne(^{3}He, t)^{20}Na reaction was investigated at various ^{3}He beam energies in the range 24–27 MeV. The $^{3}He^{++}$ beam intensity varied between 0.5 and 2.5 μA on target.

A small gas target was constructed using thin (2 μm) Ni foils as entrance and exit windows. The target was pressurized to 0.2 atm of 99.5% enriched ^{20}Ne gas, which was circulated through a sorption pump immersed in liquid nitrogen in order to purge oxygen from the system. The yield of elastically scattered ^{3}He from ^{16}O with and without the purification system showed a reduction in the oxygen contamination by more than two orders of magnitude.

The reaction products were momentum analyzed with a 100 cm broad-range magnetic spectrograph [10]). A position-sensitive proportional gas counter, backed by a section of BC-408 plastic scintillator, was placed on the focal plane of the spectrograph. The signals from the position-sensitive region allowed the determination of the momentum, p, of the reaction products along the focal plane. A clean particle identification was achieved using the energy loss, or dE/dx, signal from a second proportional region and the energy signal from the plastic scintillator. The detector is described in detail in ref. [11]). Fig. 1 shows events from a typical $^{20}Ne + {}^{3}He$ experiment projected into the two-dimensional (E, dE/dx) plane. Software gating of the different particle groups in such a projection allows a clean momentum analysis of the different reaction products.

The detector was calibrated by exposing it to 25.5 MeV ^{3}He particles which had been elastically scattered from a thin gold foil at a laboratory angle of 70°. The use of such a large deflection angle makes it possible to measure the reaction products "in reflection". The edge of the observed ^{3}He peak corresponds to scattering from the surface of the gold foil, eliminating the need for energy loss corrections. The

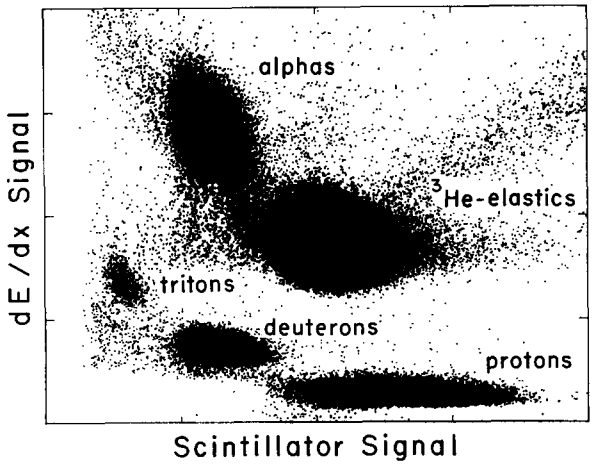

Fig. 1. Event plot from the detector system with the energy loss signal versus the energy signal from the scintillator. Tritons are seen to be clearly separated from the other particle types.

measured position on the focal plane, as determined from the peak in the timing spectrum, can then be compared to kinematic calculations of the position to establish the energy calibration for the detector.

3. Experimental results

The level structure of ^{20}Na was studied from the ground state to excitation energies of 3.6 MeV. Since the detector covers only about $\frac{1}{8}$th the length of the focal plane, the data were taken in three overlapping momentum ranges. A total of 14 levels, including the ground state, were detected, with eight states below and six states above the proton threshold at 2.199 MeV. Fig. 2 shows a set of typical triton spectra, taken with a 25.5 MeV ^{3}He beam at a laboratory angle of $\theta = 25°$. The overall energy resolution of 80 keV arises mainly from the straggling of the beam particles in the entrance foil of the gas target. The spectra were fitted using gaussian peak shapes and quadratic backgrounds, and the excitation energies of the observed states were calculated by including corrections for the energy lost within the gas target. Such calculations, when applied to the measured position of the known ground state, predicted the location of the ground state within the experimental errors (±8 keV), so that the excited states can be considered to be measured relative to the ground state. The energy for an excited state was determined by averaging the values obtained at all the measured angles. The errors in the excitation energies follow from the uncertainties in the fitting as well as from the standard deviations of the average values. The level structure of ^{20}Na, so obtained, is shown in fig. 3 in comparison with the well-known states in the mirror nucleus ^{20}F [ref. [12])]. There are discrepancies between these results and the results of our first attempt, most noticeably the disappearance of the previously reported level at an excitation energy

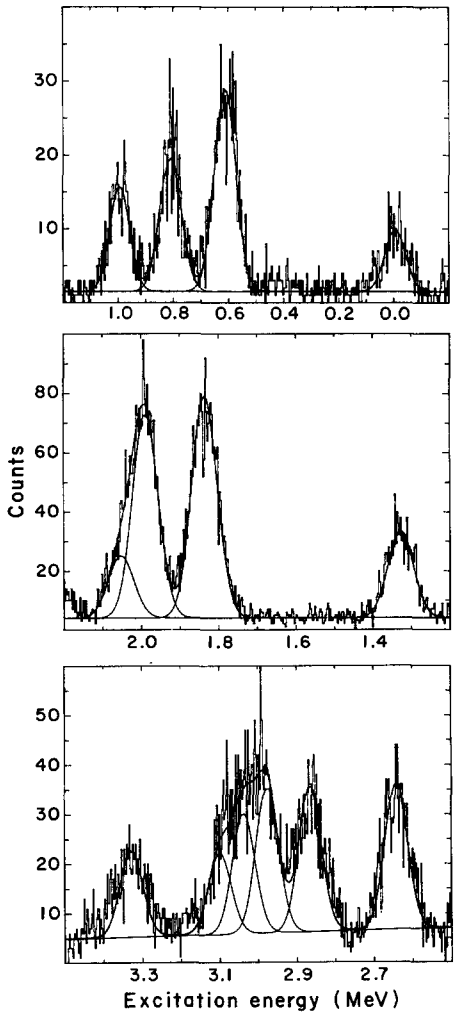

Fig. 2. A set of typical spectra covering the excitation range in ^{20}Na up to 3.5 MeV. The data were obtained at a bombarding energy of 25.5 MeV and a laboratory angle of 25°.

of 2.57 MeV (see table 2). The improvements made in particle identification and in the elimination of oxygen contamination since the first attempt are responsible for the elimination of this spurious level.

Angular distribution measurements were made over the center-of-mass angle range $\theta_{c.m.} = 7°-55°$ in steps of 5°(lab). The measured yield was normalized to the collected charge and corrected for variation of the solid angle of the spectrograph with focal surface position as well as variations in the effective pathlength in the gas cell [13]).

DWBA calculations were performed using the code DWUCK4 [14]) to obtain information about possible spin and parity assignments for the observed states. For

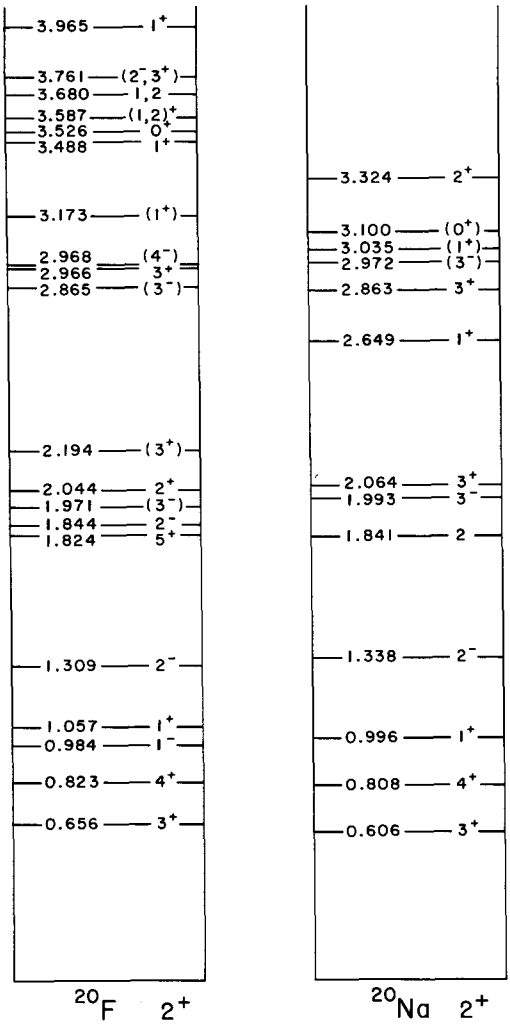

Fig. 3. Observed level sequence in ^{20}Na in comparison with the known states in the mirror nucleus ^{20}F. The $^{19}Ne+p$ threshold is at 2.199 MeV.

the analysis of (^{3}He, t) charge exchange reactions, an effective interaction in terms of the one-pion exchange potential (OPEP) and a Yukawa potential was used as suggested in ref. [15]). Initial optical-model parameters were taken from ref. [16]) and adjusted by optimizing the DWBA fit to the angular distribution for the transition to the ground state ($J^\pi = 2^+$) in ^{20}Na. The resulting optical-model parameters used in all fits are listed in table 1. Fig. 4 shows the angular distribution measurements for the observed bound states in ^{20}Na together with the results of the DWBA calculations. The data can be fitted fairly well assuming various values for the l-transfer to the populated bound states. No unambiguous spin and parity assignment

TABLE 1

Optical-model parameters used in the DWBA calculations in the nomenclature of ref. [14])

V_R (MeV)	r_R (fm)	a_R (fm)	V_I (MeV)	r_I (fm)	a_I (fm)
−180.3	1.15	0.71	−21.3	1.61	0.85

is therefore possible on the basis of the angular distribution data only. Therefore the choice of the possible l-transfer for the DWBA fits was mainly guided by the known level structure of the mirror nucleus ^{20}F [ref. [12])] shown in fig. 3. Most of the fits adequately represent the data and support these assignments. The DWBA calculation for the level at 0.996 MeV seems to favour a $J^\pi = 1^+$ assignment. The analog assignment for the closely spaced levels between 1.8 MeV and 2.1 MeV excitation energy is uncertain. Therefore the angular distribution of the three observed levels at 1.841, 1.993 and 2.064 MeV have been fitted by assuming various possible spin and parity assignments $2^+, 2^-, 3^+, 3^-, 5^+$ suggested by the observed level scheme in ^{20}F. Fig. 4 shows the best DWBA fits obtained for the various spin

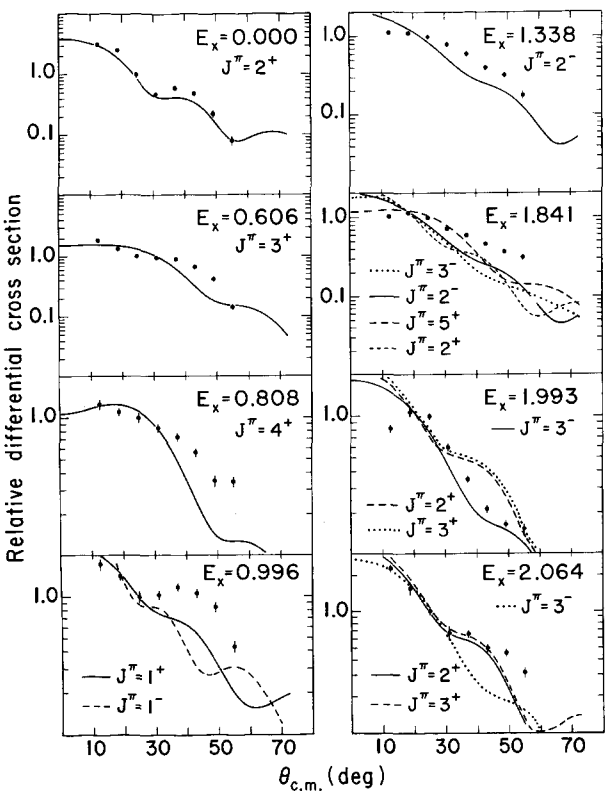

Fig. 4. DWBA analysis of the $^{20}Ne(^3He, t)$ angular distributions to the bound states in ^{20}Na.

and parity values. On the basis of these fits an $J^\pi = 3^-$ assignment is made for the level at 1.993 MeV. The DWBA results for the levels at 1.841 and 2.064 MeV are ambiguous and would be equally well explained by a $J^\pi = 2^+, 2^-$ or 5^+ and a $J^\pi = 2^+, 3^+$ assignment, respectively (see table 2). Recent unpublished high-resolution $^{20}Ne(^3He, t)^{20}Na$ measurements indicate a doublet structure for both states [17,18]). This suggests five levels in this excitation range, in agreement with the number of levels in the mirror nucleus.

Of the six levels observed above the proton threshold, the three states at 2.972, 3.035 and 3.100 MeV are unresolved. For this reason, no reliable spin and parity assignment can be made for these three levels on the basis of the experimental data.

DWBA fits to the angular distributions of the three remaining unbound states are shown in fig. 5. For the level at 2.649 MeV, fits are shown for the feasible spin and parity values $J^\pi = 1^+, 3^+, 3^-$. The results clearly indicate a $J^\pi = 1^+$ assignment for this level and rule out the other possibilities of $J^\pi = 3^+, 3^-$. This assignment is in good agreement with the result of ref. [9]). For the level at 2.863 MeV, DWBA fits to the angular distribution are shown assuming $J^\pi = 3^+, 3^-, 4^-$, based on the analog structure of ^{20}F in this excitation range. The fit for $J^\pi = 3^+$ gives the best representation of the data, again consistent with the results in ref. [9]). For the level at 3.324 MeV fits are shown for $J^\pi = 0^+$, 1^+ and 2^+. While the $J^\pi = 0^+$ assignment is clearly ruled out by the fit, no distinction can be made between $J^\pi = 1^+$ and $J^\pi = 2^+$, since both

TABLE 2

Comparison of the present experimental results with previous observations. Energies given in MeV, energy uncertainties in keV

E_x [ref. [12])]	E_x (^{3}He, t) [9])	J^π	E_x (p, n) [9])	J^π	E_x (present)	J^π [b])
0.591 (12)	0.600 (15)	$(3, 4, 5)^+$	0.580 (15)	3^+	0.606 (13)	3^+
0.768 (08)	0.802 (15)	$(3, 4, 5)^+$	0.790 (15)	4^+	0.808 (11)	4^+
0.958 (08)	0.990 (15)	$(1, 2, 3)^+$	0.993 (15)	1^+	0.996 (12)	1^+
1.010 (14)	-		-		-	
1.310 (10)	1.347 (15)	$(2, 3, 4)^-$	1.353 (15)	(2^-)	1.338 (14)	2^-
1.820 (20)	1.832 (15)	$(2, 3, 4)^-$	1.843 (15)	(2^-)	1.841 (11)	$2^\pm$
1.910 (20)	1.967 (20)	$(2, 3, 4)^-$	2.016 (20)	(3^-)	1.993 (12)	3^-
1.980 (20)	2.034 (20)	$(3, 4, 5)^+$	-		2.064 (16)	$(2, 3)^+$
2.570 (20)	[a])					
2.660 (20)	2.637 (15)	$(0, 1)^+$	2.651 (20)	1^+	2.649 (16)	1^+
2.880 (40)	2.842 (15)	$(3, 4, 5)^+$	2.852 (20)	$(2, 3)^+$	2.836 (12)	3^+
2.960 (40)	2.967 (20)		-		2.972 (13)	
3.060 (40)	3.046 (20)	$(1, 2, 3)^+$	3.053 (20)		3.035 (15)	
3.160 (40)	-		-		3.100 (14)	
-	3.302 (30)	$(4, 5, 6)^-$	-		3.324 (11)	$(1, 2)^+$

[a]) Omitted, see discussion in text.

[b]) Spin and parity assignments are based on DWBA fits guided by the spin sequence of the mirror nucleus ^{20}F.

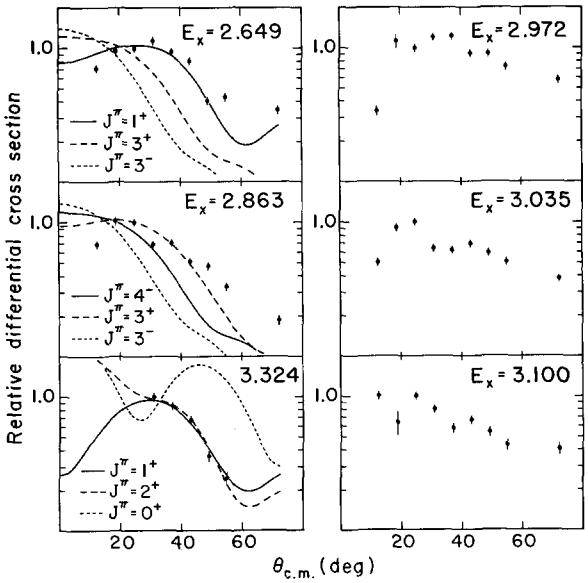

Fig. 5. Angular Distributions and DWBA fits for the unbound states in ^{20}Na. No DWBA analysis was attempted for the three unresolved levels at 2.972, 3.035 and 3.100 MeV.

correspond to an l-transfer of $l=2$. The experimental data could not be fitted by DWBA calculations assuming negative parity for the state as suggested in ref. [19]).

The excitation energies, spins, and parities of the observed levels are listed in table 2 along with the results of refs. [9,12]) for comparison.

4. Level structure of ^{20}Na

The relationship between energies in an isobaric multiplet are known to be well reproduced by the isobaric-mass-multiplet equation (IMME) [20,21])

$$E(\nu, T, T_z) = a(\nu, T) + b(\nu, T)T_z + c(\nu, T)T_z^2 . \quad (1)$$

In the following we discuss the level and spin assignments in ^{20}Na based on this equation as used in the combination with experimental and calculated values for the a-, b- and c-coefficients.

All of the positive-parity states in ^{20}F, except for the second 1^+ state, are well described in the $(2s_{1/2}, 1d_{5/2}, 1d_{3/2})$ (sd) model space with the interactions of Wildenthal [22,23]). For the negative-parity states and the second 1^+ state we will make use of wave functions in the $(1p_{1/2}, 2s_{1/2}, 1d_{5/2})$ (psd) model space obtained with the interaction of Reehal and Wildenthal [24,25]). All calculations were carried out with the OXBASH shell-model code [26]).

The calculated energies are compared with the experimental values in ^{20}F and ^{20}Ne in table 3. The positive-parity states are in excellent agreement with the

TABLE 3

Comparison of the theoretical excitation energies from shell-model calculations for the $A=20$, $T=1$ triplet with the semi-empirical results using the IMME mass equation and with the present experimental results. All enegies (in MeV) are relative to the $T=1$ ground state

E_x $A=20$ [a]	J^π	E_x ^{20}Ne (exp.)	J^π	E_x ^{20}F (exp.)	J^π	E_x ^{20}Na (b-coeff.) [b]	E_x ^{20}Na (c-coeff.) [b]	J^π	E_x ^{20}Na (exp.)	J^π_x (adopt.)
0.598	3^+	0.610	3^+	0.656	3^+	0.626	0.606	3^+	0.606	3^+
0.738	4^+	0.816	4^+	0.823	4^+	0.782	0.805	4^+	0.808	4^+
1.048	1^+	0.988	1^+	1.057	1^+	1.055	0.951	1^+	0.996	$1^\pm$
0.485	1^-	0.996	1^-	0.984	1^-		0.970	1^-		
0.680	2^-	1.327	2^-	1.309	2^-		1.323	2^-	1.338	2^-
1.743	5^+			1.824	5^+	1.790		5^+	1.85 [c]	5^+
1.197	2^-	1.824	2^-	1.844	2^-		1.806	2^-		
2.095	2^+	1.947	2^+	2.044	2^+	1.990	1.830	2^+	1.841	$2^\pm$
1.282	3^-	1.982	3^-	1.971	3^-		1.989	3^-	1.993	3^-
2.198	3^+	2.127	(3^-)	2.194	(3^+)	2.142	2.116	3^+	2.064	3^+
3.300	1^+	2.897 [d]	1^+	3.173	1^+		2.697	1^+	2.649	1^+
2.079	3^-			2.865	(3^-)	2.883		3^-	2.972	(3^-)
2.896	3^+			2.966	3^+	2.786		3^+	2.836	3^+
1.980	4^-			2.968	4^-					
3.348	1^+	3.210	1^+	3.488	1^+	3.435	3.036	1^+	3.035	(1^+)
3.490	0^+	3.368	0^+	3.526	0^+	3.415	3.080	0^+	3.100	(0^+)
3.361	2^+	3.607	2^+	3.587	$(1,2)^+$	3.477	3.565	2^+	3.324	(2^+)
3.484	3^+			3.761	$(2^-,3^+)$					

[a]) The positive-parity states (except for the second 1^+ state) are based on the sd model space with the interaction of Wildenthal [22,23]). The negative-parity states and the second 1^+ state are based on the psd model space with the interaction of Reehal and Wildenthal [25]).

[b]) The energies in ^{20}Na estimated on the basis of the calculated b- and c-coefficients.

[c]) Ref. [26]).

[d]) ($T=1$), ref. [12]).

experiment and always well within the global 185 keV r.m.s. difference between experiment and theory obtained for the entire sd shell [22]). The negative parity states are systematically 500–1000 keV too low in the psd theory. Deviations of this size are typical in the psd model space [24,25]).

Next in table 3 we give the estimated excitation energies for positive parity states in ^{20}Na based on the known energies in ^{20}F and the calculated b-coefficients.

$$E_x(^{20}\mathrm{Na}, \nu) = E_x(^{20}\mathrm{F}, \nu) - 2[b(\nu) - b(2^+, \text{g.s.})] . \quad (2)$$

The b-coefficients were obtained from the global empirical isospin nonconserving interactions (INC) of Ormand and Brown [21]) for the sd model space. The average r.m.s. deviation between the calculated b-coefficients and the experimental values for the sd-shell cases considered in ref. [21]) was 27 keV. Based on this, we would expect the calculated excitation energies to be good to about 76 keV.

However, as will be important for latter comparisons, an exceptional case is the first excited $\frac{1}{2}^+$ state in ^{17}F–^{17}O. The anomalously large downward shift for this $l=0$

state in ^{17}F due to its small binding energy is well known. The empirical INC interaction considered in ref. [21]) does not take these small binding effects into account and should be used with the expected confidence of 27 keV only for well bound states.

When the energies of states are known in both ^{20}F and ^{20}Ne, it is better to estimate the energies of the analog states in ^{20}Na from the relation:

$$E_x(^{20}\mathrm{Na}, \nu) = 2E_x(^{20}\mathrm{Ne}, \nu) - E_x(^{20}\mathrm{F}, \nu) + 2[c(\nu) - c(2^+, \mathrm{g.s.})], \qquad (3)$$

where the calculated c-coefficient for the different levels is based on the isospin nonconserving interactions of ref. [21]) as used in the model spaces discussed above [see also footnote [a]) in table 3]. The average r.m.s. deviation between the calculated c-coefficients and the experimental values for the sd-shell cases considered in ref. [21]) was 9 keV. Based on this, we expect the derived excitation energies to be good to about 25 keV. The small binding effects mentioned above should give a much smaller error in this case since most of the effect is automatically taken into account by making use of the experimental shift between ^{20}F and ^{20}Ne. We see in fact that the estimated energies listed in table 3 generally agree within the expected error of 25 keV with levels observed in the present experiment.

For the bound states, the overall agreement between these calculations and the experimental results is excellent, considering that the doublet near 1 MeV and the triplet near 1.8 MeV were not resolved [17,18]) within the resolution of this experiment. The predicted excitation energy of 1.764 MeV for the $J^\pi = 5^+$ state agrees well with a level at 1.85 ± 0.21 MeV, observed in ^{19}F(p, π^-)^{20}Na, which is very selective for high-spin states [27]).

The calculations predict five unbound states with excitation energies $E_x < 3.6$ MeV. The $J^\pi = 3^+$ state, predicted at an excitation energy of 2.786 ± 0.05 MeV agrees well with the observed 3^+ level at 2.836 ± 0.012 MeV. The three unresolved states near 3.0 MeV excitation energy can be identified with the predicted 3^-, 1^+, 0^+ states at 2.883, 3.036 and 3.080 MeV. An additional high spin state ($J = 6, 7$) at 3.01 MeV, suggested in ref. [27]), has not been taken into consideration. A $J^\pi = 2^+$ state is predicted by the shell-model calculation based on the sd model space at an excitation energy of 3.361 MeV. The estimated excitation energy of 3.565 MeV for this state in ^{20}Na based on the known energies in ^{20}F and ^{20}Ne is considerably higher than the observed level energy at 3.324 ± 0.011 MeV (1^+, 2^+). However the 2^+ assignment for this level in ^{20}F and ^{20}Ne is not certain.

Shell-model calculations in an sd-shell configuration space for $A = 20$, $T = 1$ nuclei predict only two $J^\pi = 1^+$ states in the excitation range below 3.5 MeV [refs. [23,24])] (see table 3). These two levels, at 11.26 MeV and 13.48 MeV in ^{20}Ne, were seen strongly in a recent (p, p′) experiment [28]) in agreement with shell model predictions, confirming the sd-shell structure of these states. In ^{20}Na these two levels are identified with the first and the third observed 1^+ states comparing the estimated and observed excitation energies. The predicted and observed large downward shift of the third 1^+ state and also the first 0^+ state, similar in magnitude to that in ^{17}F, confirms also

the $^{19}Ne+2s_{1/2}$ ($l=0$) nature of these states. (It is not particularly critical that the states are slightly unbound since there is a Coulomb barrier of about 3.5 MeV.)

The second observed $J^\pi = 1^+$ state at an excitation energy of 2.649 MeV cannot be explained in terms of the sd-shell structure. The analog nucleus ^{20}Ne shows three $J^\pi = 1^+$ states at 11.26 MeV, 13.17 MeV and 13.48 MeV. Considering only the two upper levels, $^{19}F(d, n)^{20}Ne$ measurements [29]) indicate a $T=1$ assignment for the 13.484 MeV state and a tentative $T=1$ assignment for the 13.171 MeV level. The mirror nucleus ^{20}F also clearly shows two $J^\pi = 1^+$ levels at 3.173 and 3.488 MeV [ref. [12])], where the $J^\pi = 1^+$ assignment is based on $^{18}O(^3He, p)^{20}F$ [ref. [30])] and $^{21}Ne(t, \alpha)^{20}F$ [ref. [31])] measurements. The state at 3.488 MeV has also been observed in a thermal neutron capture reaction $^{19}F(n, \gamma)^{20}F$ [ref. [32])] and in an investigation of the β-decay of ^{20}O [ref. [33])], and this level has been identified as the predicted second $J^\pi = 1^+$ state [23,24]) with a $(2s, 1d)^4$ shell configuration. Neither of these experiments gives an indication for the second $J^\pi = 1^+$ state at 3.173 MeV. However, it was proposed in ref. [33]) that the weak γ-transition of $E_\gamma = 3.428$ MeV, observed in ref. [32]), can be identified with the primary feeding of the 3.173 MeV state. This implies that the level is only weakly populated (or not populated at all) in the γ-decay following the thermal neutron capture on ^{19}F as well as in the β-decay of ^{20}O. In ref. [33]) this state has therefore been identified as the lowest lying $2\hbar\omega$ $J^\pi = 1^+$ core excited intruder state of the $(1p)^{-2}(2s1d)^6$ configuration space (6p2h), with little or no mixing amplitude with the $0\hbar\omega$ $J^\pi = 1_2^+$ $(2s1d)^4$ state (4p0h).

Our results suggest an identification of the second observed $J^\pi = 1^+$ level in ^{20}Na at 2.649 MeV as the mirror state to the discussed $J^\pi = 1^+$ intruder state at 3.173 MeV in ^{20}F. The estimated excitation energy 2.697 MeV for the state in ^{20}Na based on the level energies in ^{20}F and ^{20}Ne and the calculated c-coefficient for a psd-space configuration, is in excellent agreement with the observed excitation energy of 2.649 MeV.

Virtually no $l=0$ single-particle strength is expected for a $J^\pi = 1^+$ core excited state [30]) as observed for the 3.173 MeV level in ^{20}F [ref. [34])]. From the known $^{19}F(d, p)$ angular distribution an upper limit for the $l=0$ spectroscopic factor of $S \leq 0.0001$ can be estimated. The analog 13.171 MeV state in ^{20}Ne shows an s-wave component in the $^{19}F(d, n)^{20}Ne$ single-particle transfer [28]). The $l=0$ strength, however, is very weak compared to the other observed $J^\pi = 1$, $T=1$ states in ^{20}Ne and can most likely be explained with a small $T=0$ isospin mixing component.

5. Stellar reaction rate for $^{20}Ne(p, \gamma)^{20}Na$

Using the level assignments discussed above, the proton and gamma partial widths, Γ_p and Γ_γ, can be estimated for the unbound states in ^{20}Na. The γ-decay of the positive-parity mirror (4p0h) states in ^{20}F is determined predominantly by M1-transitions with little or no E2 mixing [12]), except for the E1 decay of the (6p2h)-intruder state at 3.173 MeV to the fourth excited state at 0.98 MeV, which has $J^\pi = 1^-$

with a predominant (5p1h) configuration. The negative-parity level at 2.865 MeV decays by 100% E1 transition to the ground state. The transition matrix elements for M1 and E1 transitions in ^{20}F are the same for the corresponding γ-transitions in the mirror nuclei and were adopted to calculate the γ-partial widths Γ_γ of the proton unbound states in ^{20}Na (see table 4).

The experimental single-particle spectroscopic factors, $S(l)$, of the states between 2.5 and 3.5 MeV in ^{20}F [ref. [34])] agree well with the theoretically calculated spectroscopic factors for the $A=20$, $T=1$ states predicted in that excitation range [26]). We therefore adopted the experimental values to calculate the proton widths of the unbound mirror levels in ^{20}Na, using the procedure described in ref. [4]). For the intruder level at an excitation energy of 2.649 MeV, the proton partial width Γ_p is determined by the small, $S(l=2)=0.0063$, $l=2$ single-particle component with a possible very small additional $l=0$ component $S(l=0)\leq 0.0001$. The resulting proton width of $\Gamma_p=\Gamma_{p_0}+\Gamma_{p_2}$ with $\Gamma_{p_2}=0.078$ eV and $\Gamma_{p_0}\leq 0.09$ eV is therefore much smaller than the 6.8 keV suggested in refs. [4,19]). Spectroscopic factors and partial widths for the observed proton unbound levels in ^{20}Na are listed in table 4.

The stellar reaction rate for ^{19}Ne(p, γ)^{20}Na is determined by resonant and nonresonant reaction contributions [4]). The resonant reaction rate can be calculated from the resonance strengths $\omega\gamma_r$ (in MeV), also listed in table 4, using the relation [35]),

$$N_A\langle\sigma v\rangle_{res}=1.65\times 10^2 T_9^{-3/2}\sum_r \omega\gamma_r \exp\left(-11.605E_r/T_9\right), \qquad (4)$$

where E_r is the resonance energy (in MeV) in the center-of-mass system and T_9 is the temperature (in 10^9 K). The contributions of the single resonances are shown in fig. 6. The resonant reaction rate in the temperature range $T_9\leq 1$ is clearly dominated by the influence of the $J^\pi=1^+$ intruder state at 2.649 MeV. At higher temperatures, the resonant reaction rate is determined by the resonant contributions

TABLE 4

^{19}Ne(p, γ)^{20}Na resonance parameters for the observed proton unbound states in ^{20}Na

E_x (MeV)	E_r (MeV)	J^π [a])	l	S_{th} ($A=20$)	S_{exp} [34]) (^{20}F)	Γ_p (eV)	L	Γ_γ (eV)	$\omega\gamma$ [b]) (meV)
2.649	0.450	1^+	0		≤ 0.0001	≤ 0.092			
			2		0.0063	0.078	E1	0.0093	6.23
2.836	0.637	3^+	2	0.007	0.0054	6.120	E1	0.0090	15.95
2.972	0.773	3^-	3		0.0006	0.120	M1	0.0390	51.19
3.035	0.837	1^+	0	0.33	0.40	1.93×10^4	M1	0.010	7.50
3.100	0.901	0^+	0	0.56	0.28	2.95×10^4	M1	0.015	3.75
3.324	1.162	2^+	2	0.004	0.008	2.71×10^1	M1	0.014	17.50

[a]) The spin and parity assignments for the unbound states are based on the results of the DWBA analysis shown in fig. 5 and on the results of the shell-model calculations presented in table 3.

[b]) $\Gamma_\gamma \ll \Gamma_p$ for all the discussed cases, therefore the resonance strengths $\omega\gamma=\omega\Gamma_\gamma$ do not depend critically on the assigned l-values and proton widths, but only on the γ-partial widths. The expected uncertainty is within a factor of three.

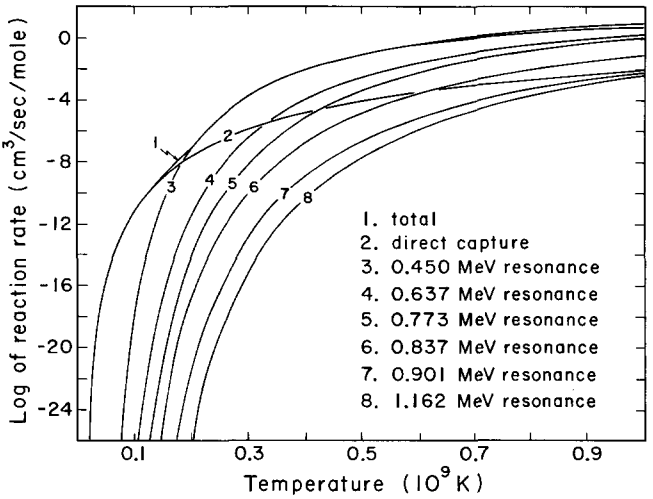

Fig. 6. Nonresonant and resonant contributions to the reaction rate of $^{19}Ne(p, \gamma)^{20}Na$ as a function of temperature.

of the $J^\pi = 3^+, 3^-$ states at 2.836 and 2.972 MeV. The contribution of higher excited levels is negligible.

Considerable contributions to the reaction rate from the low-energy tails of broad resonances were calculated in ref. [4]), where the contributions were dominated by the low-energy tail of a proposed $J^\pi = 1^+$ resonance at $E_r = 0.68$ MeV with a width of $\Gamma = 6.8$ keV [see fig. 1 in ref. [4])]. For the actually observed $J^\pi = 1^+$ level at an excitation energy of 2.649 MeV, corresponding to a resonance energy of $E_r =$ 0.45 MeV, the total width is much smaller than that used in ref. [4]) because of the reduced proton penetrability through the Coulomb barrier. Therefore, the tail contribution to the reaction rate does not remain unchanged, as assumed in ref. [19]), but is only determined by the low-energy tail of the second $J^\pi = 1^+$ state at a resonance energy of $E_r = 0.834$ MeV. The resulting tail rate is reduced by one order of magnitude, as compared to the tail rate of ref. [4]), and can therefore be neglected.

The nonresonant direct-capture contribution to the reaction rate of $^{19}Ne(p, \gamma)^{20}Na$ has been taken from ref. [4]). However, it should be pointed out that in eq. (8) of ref. [4]) a $T_9^{1/3}$ term was omitted. The equation should read

$$N_A\langle\sigma v\rangle_{dc} = 1.713 \times 10^6 T_9^{-2/3} \exp(-19.38 T_9^{1/3}) \times (1 + 2.12 \times 10^{-2} T_9^{1/3} + 1.30 \times 10^{-1} T_9^{2/3} + 1.92 \times 10^{-2} T_9 + 3.86 \times 10^{-2} T_9^{4/3} + 1.47 \times 10^{-2} T_9^{5/3}) . \quad (5)$$

The direct-capture contribution is also shown in fig. 6. As already pointed out in ref. [4]) the direct-capture term dominates the reaction rate in the low-temperature region $T_9 \leq 0.2$, while at higher temperatures the rate is determined by the resonant components.

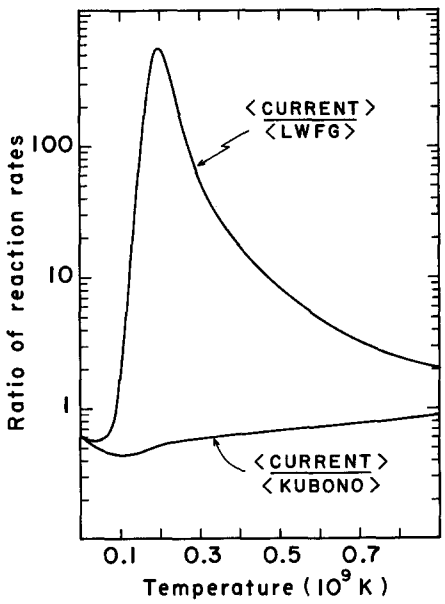

Fig. 7. Comparison of the present reaction rate for $^{19}Ne(p, \gamma)^{20}Na$ with the results of previous calculations.

Fig. 7 compares the reaction rate with the result of previous work. The present total rate

$$N_A\langle\sigma v\rangle_{tot} = N_A\langle\sigma v\rangle_{res} + N_A\langle\sigma v\rangle_{dc} \quad (6)$$

is slightly smaller at $T_9 \leq 0.15$ than the results of ref. [4]), adopted in ref. [19]). This is mainly explained by the omission of the tail contribution of the broad resonances at low energies.

At higher temperatures the present rate is considerably higher than suggested in ref. [4]) because of the influence of the newly observed level at 2.649 MeV. The new rate, however, is about a factor of two smaller than proposed in ref. [19]), where the influence of this level was taken into account. Taking the resonance parameters from ref. [4]) without modification, as was done in ref. [19]), neglects the strong energy dependences of the partial widths and is responsible for the observed differences.

It is important to note that the new rate, as determined from these data, is considerably enhanced in the temperature range $0.2 \leq T_9 \leq 0.3$, as compared to previous theoretical estimates [4]) (see fig. 7). This enhancement indicates the possibility of significant "break-out" from the hot CNO cycle at temperatures lower than previously accepted, with consequences for a variety of sites of astrophysical importance.

This work was supported by the National Science Foundation Grant PHY 86-11210. The authors thank Prof. N. Clarke and in particular Prof. P.D. Parker for many helpful discussions and suggestions.

References

1) J. Audouze, J.W. Truran and B.A. Zimmerman, Astrophys. J. **184** (1973) 493
2) R.K. Wallace and S.E. Woosley, Astrophys. J. Suppl. **45** (1981) 389
3) M. Wiescher, J. Görres, F.-K. Thielemann and H. Ritter, Astron. Astrophys. **160** (1986) 56
4) K.H. Langanke, M. Wiescher, W.A. Fowler and J. Görres, Astrophys. J. **301** (1986) 639
5) P. Magnus, M.S. Smith, P.D. Parker, R.E. Azuma, C. Campell, J.D. King and J. Vise, Nucl. Phys. **A470** (1987) 206
6) F. Ajzenberg-Selove, Nucl. Phys. **A300** (1978) 1
7) F. Ajzenberg-Selove, Nucl. Phys. **A392** (1983) 1
8) L.O. Lamm, C.P. Browne, J. Görres, M. Wiescher and A.A. Rollefson, Z. Phys. **A327** (1987) 239
9) S. Kubono, N. Ikeda, M. Yasue, T. Nomura, Y. Fuchi, H. Kawashima, S. Kato, H. Orihara, T. Shinozuka, H. Ohnuma, H. Miyatake and T. Shimoda, Z. Phys. **A331** (1988) 359; in Proc. of the Int. Symposium on heavy ion physics and nuclear astrophysical problems, 1989, Singapore (World Scientific, Singapore, 1989) p. 83
10) J.D. Goss, A.A. Rollefson and C.P. Brown, Nucl. Insr. Meth. **109** (1973) 13
11) L.O. Lamm, S.M. Graff, M. Wiescher, J. Görres, C.P. Browne and U. Giesen, Nucl. Instr. Meth. **A281** (1989) 143
12) F. Ajzenberg-Selove, Nucl. Phys. **A475** (1987) 1
13) E.A. Silverstein, Nucl. Instr. Meth. **4** (1959) 53
14) F.D. Kunz (1983) unpublished
15) R. Schaeffer, Nucl. Phys. **A164** (1971) 145
16) J. Vernotte, G. Berrier-Ronsin and J. Kalifa, Nucl. Phys. **A390** (1982) 285
17) N. Clarke (1989) private communication
18) P. Parker (1989) private communication
19) S. Kubono, H. Orihara, S. Kato and T. Kajino, Astrophys. J. **344** (1989) 460
20) W. Benenson and E. Kashy, Rev. Mod. Phys. **51** (1979) 527
21) W.E. Ormand and B.A. Brown, Nucl. Phys. **A491** (1989) 1
22) B.H. Wildenthal, Prog. Part. Nucl. Phys. **11** (1984) 5
23) B.A. Brown and B.H. Wildenthal, Ann. Rev. Part. Nucl. Sci. **38** (1988) 29
24) J.B. McGrory and B.H. Wildenthal, Phys. Rev. **C7** (1973) 974
25) B.S. Reehal and B.H. Wildenthal, Part. Nucl. **6** (1973), 137
26) B.A. Brown, A. Etchegoyen and W.D.M. Rae, MSU/NSCL-Report **524** (1985)
27) Z.-J. Cao, R.D. Bent, H. Nann and T.E. Ward, Phys. Rev. **C35** (1987) 625
28) A. Willis *et al.*, Nucl. Phys. **A464** (1987) 315
29) R.C. Ritter, J.T. Parson and D.L. Bernard, Phys. Lett. **B28** (1969) 588
30) R. Medoff, L.R. Medsker, S.C. Headley and H.T. Fortune, Phys. Rev. **C14** (1976) 1
31) G.B. Liu and H.T. Fortune, Phys. Rev. **C37** (1988) 1818
32) P. Hungerford, T. von Egidy, H.H. Schmidt, S.A. Kerr, H.G. Börner and E. Monnand, Z. Phys. **A313** (1983) 339
33) D.E. Alburger, G. Wang and E.K. Warburton, Phys. Rev. **C35** (1987) 1479
34) H.T. Fortune and R.R. Betts, Phys. Rev. **C10** (1974) 1292
35) W.A. Fowler, G.R. Caughlan and B.A. Zimmerman, Ann. Rev. Astron. Astrophys. **13** (1975) 69